Acta Technica *62* (2017), No. 6B, 889–898

A numerical simulation method for machine finite element analysis

Tiantao Feng[1], Guiju Fan[1,*], Xiaohui Zhang[1]

Abstract. In order to improve the research and analysis precision of aluminum alloy plastic flow thermally coupled welding process, the finite element analysis method of aluminum alloy plastic flow thermally coupled welding process is proposed. Firstly, the basic theory of finite element for rigid viscoplasticity of aluminum alloy is given, and the finite element solution equations on velocity increment are obtained with the fact that the basic theory is Markov variational principle; secondly, the analysis model for finite element field of aluminum alloy plastic flow thermal coupling is given to have given two models, namely, single-layer aluminum alloy plastic flow thermal coupling and multi-layer aluminum alloy plastic flow thermal coupling with finite length diameter; finally, the effectiveness of the algorithm is verified by simulation experiments.

Key words. Aluminum alloy, Plastic flow, Thermal coupling, Finite element.

1. Introduction

As a kind of less cutting process, the bulk forming of aluminum alloy is widely used in manufacturing industry because of the characteristics of its high quality and high efficiency. With the rapid development of numerical simulation technology and the further deepening understanding of aluminum alloy flow law in recent years, numerical simulation technology plays an increasingly important role in aluminum alloy bulk forming. By using numerical simulation, the designers are assisted to optimize the parameters, in order to achieve defect-free design.

In the plastic deformation of aluminum alloy, the temperature has a great impact on the deformation. Due to the uneven deformation of the workpiece during the plastic processing, the heat generated by the deformation is differently distributed in the parts of the workpiece. There is not only heat transfer between workpiece and mould and thermal radiation and heat convection between workpiece and environment; but also plastic deformation work and friction work on the contact surface

[1]Shandong Provincial Key Laboratory of Horticultural Machineries and Equipments, Shandong Agriculture University, Taian, China
Corresponding author

of workpiece and mould are translated into thermal energy, so that the temperature in the workpiece and mold is unevenly distributed. Uneven temperature field will affect the quality of the product, or even form a defect. Therefore, it is necessary to combine the deformation flow and the thermal effect to carry on the coupling analysis.

Aimed at the analysis problem of aluminum alloy plastic flow thermally coupled welding process, the effective analysis of aluminum alloy plastic flow thermally coupled welding process has been achieved with the finite element of thermal radiation field to carry out analysis under the condition of thermal coupling. The experiment results have verified the effectiveness of the method proposed.

2. Basic theory of finite element for rigid viscoplasticity of aluminum alloy

For forming problems of aluminum alloy with large deformation, the deformation aluminum alloy shall be deemed as a rigid plastic body, so at this time, the material shall meet the following assumptions: the elastic deformation of the material shall be excluded; the bulk shall be incompressible; the materials shall be isotropic bodies; the bulk force and inertia force shall be excluded; the material flow shall obey flow rules of Levy-Mises.

When plastic deformation happens to rigid-plastic materials, the basic equations and basic conditions of the following plastic mechanics shall be met: (1) equilibrium differential equation: $\sigma_{ij,i} = 0$; (2) relationship between speed-strain rate: $\varepsilon_{ij} = \frac{1}{2}(u_{i,j}+u_{j,i})$; (3) constitutive equation: $\varepsilon_{ij} = \lambda\sigma'_{ij}$ and $\lambda = 3\overline{\xi}/2\overline{\sigma}$; (4) yield criterion: $\frac{1}{2}\sigma'_{ij}\sigma'_{ij} = k^2$; (5) incompressible conditions of bulk: $\varepsilon_v = \varepsilon_{kk} = 0$; (6) boundary conditions: $\sigma_{ij} = \overline{F}_i$.

The basic theory of rigid-plastic finite element is the variational principle of Markov. In the kinematically admissible velocity field meeting the velocity condition, the coordination equation and the incompressible volume condition, the real velocity field must be the minimum value acquired by the following functional. The functional of penalty function method widely used can be expressed as:

$$\pi = \int_v = \overline{\sigma}\overline{\varepsilon}dv + \frac{k}{2}\int_v \overline{\varepsilon}dv - \int_{S_F} F_i u_i dS\,. \tag{1}$$

In the formula, k is the penalty factor, the true solution of which can be acquired when $\delta\pi = 0$. The solution equation set concerning velocity increment for finite element can be acquired by carrying out variation and linear treatment on the above formula:

$$[S][\Delta U] = \{R\}\,. \tag{2}$$

In the formula, $[S]$ is the stiffness matrix, $\{R\}$ is the load vector sum and $[\Delta U]$ is the increment vector for the node rate. This linear equation is a general formula of rigid-plastic finite element method, in which a variety of mechanics field quantity can be acquired with the solution of Newton-Raphson iteration method.

3. Finite element field analysis of heat transfer of aluminum alloy

3.1. Distribution of heat transfer field

In general, the ratio between the length and diameter of the heat transfer field is infinite if it is in an ideal state, the heat transfer field in general is plasticized with a single layer method and if the theorem is calculated in accordance with Savart-Biot, the field strength inside heat transfer field can be acquired, in which the form of expression B_0 is:

$$B_0 = \mu_0 n_0 I/2I\,. \tag{3}$$

In formula (3), the parameter $2l$ is an aluminum alloy body in any section of aluminum alloy; parameter n_0 is the strength of heat transfer field contained in the length of the aluminum alloy body selected. Aimed at the ideal heat transfer field studied to carry out the field induction analysis, the following research results can be acquired:

(1) Because the heat transfer field in the ideal state meets the limiting conditions, and the field strength calculated based on this condition is also the limiting characteristic case, but in the real application environment, the heat conduction field in the ideal state does not exist, so the state of heat transfer field is approximate to limit state generally by setting the conditions.

(2) The internal field of heat transfer in the ideal state can acquire synchronous and even field distribution along radial and axial directions and a more ideal test result can be acquired based on the field analysis of heat transfer in the ideal state above and heat transfer field approximate to be in the ideal state as the plastic analysis method of aluminum alloy.

3.2. Field distribution analysis of single-layer aluminum alloy

If the heat transfer field of aluminum alloy studied has a single-layer structure, and the length parameter of the heat transfer field is $2l$, the total plastic strength is n_1. The distribution form of the field strength in the axial direction can be acquired by further using Savart-Biot calculation law, which is:

$$B_x = \frac{\mu_0 n_1 I}{2l}\frac{l}{2}\left[\frac{x+l}{\sqrt{r^2+(x+l)^2}} - \frac{x-l}{\sqrt{r^2+(x-l)^2}}\right]. \tag{4}$$

According to formula (2), if the value of l/r is limited, the field strength in heat transfer field along the axial direction is related to the value of x in the axial direction of coordinate, and if $x = 0$ or $x = \pm l$ is satisfied, the value of l/r is limited, and meanwhile it can be known that the field distribution in the axial direction of heat transfer field is not uniform, so aimed at the case of limited value of tl/r, it is divided into two cases to analyze the field distribution in heat transfer field:

(1) To analyze the effect of the value of l/r on the field strength along the axis

of the heat transfer field. If $x = 0$ is satisfied, that is, it is located in the central axial area of the heat transfer field, the field strength of this location area B can be calculated with formula (4):

$$B = \frac{\mu_0 n_1 I}{2l} - \frac{(l/r)}{\sqrt{l + (l/r)^2}} = B_0 \beta_0 \,. \tag{5}$$

In formula (5), B_0 is the value of field strength generated by heat transfer field in the ideal state; β_0 is the attenuation coefficient of the field strength along the axial direction of heat transfer field, in which this parameter value is usually chosen as $\beta_0 < 1$. If the computational formula of change amplitude α by comparing the true strength of field induction in central axial area with ideal strength of induction in ideal spiral heat transfer heat under ideal state is:

$$\alpha = (B_0 - B)/B_0 = f(l/r) = (1 - \beta_0) \times 100\% \,. \tag{6}$$

According to formula (6), it can be known that the function relationship existing in the ratio between change amplitude α and l/r can be expressed as: if $l/r > 3$, the attenuation coefficient of the field strength in the axial direction can reach 5%, if $l/r > 5$, in this case, the attenuation coefficient α of the field strength in the axial direction is <1%, in which case its working condition is in the ideal working conditions and is an ideal heat transfer field.

(2) To analyze the value of l/r for the axial distribution characteristcis of aluminum alloy of the field strength along the entire aluminum alloy. According to formula (7), it can be known that the strength component B_x of field strength along the axis on the heat transfer field is a function of x, which is inconsistent with the central strength value of the field induction. If $x = \pm l$ is true, the section strength value B_{xl} of field induction generated by heat transfer field at both ends is calculated as:

$$B_{xl} = \frac{B_0 \beta_0}{2} \,. \tag{7}$$

According to formula (5), it can be known that the axis component of field intensity at the end position of the heat transfer field is 1/2 of the field strength value at the center of the axis, which is unrelated to the value of l/r, but related to the value of l/r of the induction strength between the center of the axis and both ends. It can be known by calculation that the larger the calculated value of l/r is, the better the stability of the field strength presented in the heat transfer field is; When the calculated value of l/r tends to be infinite, the even distribution field in each direction will be generated in the heat transfer field.

3.3. Analysis of multi-layer heat transfer field

In the real application scenario, the heat transfer field used is usually multi-layer, and the internal distribution of this multi-layer heat transfer field along the axial field can be deemed as being constituted by multiple groups of heat transfer field in the axial direction. According to the previous theoretical analysis, each layer of

heat conduction field has its own inherent characteristics. Aimed at the structure of multi-layer heat transfer field studied, the inner diameter of the heat transfer field is assumed to be r_1 and its outer diameter to be r_2, then the field strength B along the axial heat transfer field and at its central position is calculated as:

$$B = \frac{\mu_0 m n_0 I}{2l} - \frac{1}{r_2 - r_1} \ln \frac{r_2 + \sqrt{r_2^2 + l^2}}{r_1 + \sqrt{r_1^2 + l}} \,. \tag{8}$$

The above formula is simplified and approximated with the first-order formula, and the specific form is as follows

$$B = \frac{\mu_0 m n_0 I}{2l} = \frac{\mu_0 n_0 I}{2l}. \tag{9}$$

In formula (9), n_0 is the strength of heat transfer field of each layer in the heat transfer field; m is the number of heat transfer layers of the heat transfer field; r_1 is the radius of heat transfer field in the innermost layer; r_2 is the radius if the heat transfer field in the outermost layer. According to formula (7), the following discussion can be acquired: (1) the total spiral strength and length of the aluminum alloy body affect the field strength at the axial position of the multi-layer heat transfer field structure, while the inner-layer length-diameter ratio of the heat transfer field does not affect the field strength at the axial position of the multi-layer heat transfer field structure; (2) the strength distribution of the single-layer heat transfer field is similar to that of the field strength at the end position of the multi-layer heat transfer field. The field strength values in both cases are half of the field strength values detected at the axial position; (3) for the multi-layer heat transfer field, the structural parameters of the length-diameter ratio are associated with the total number of layers of the heat transfer field, and meanwhile it can be known that the indicator value of length-diameter ratio (l/r_1) at the innermost layer of the heat transfer field is the largest, while the indicator value of length-diameter ratio (l/r_2) at the outermost layer of the heat transfer field is the smallest; therefore, the value range of field strength evenly distributed in the multi-layer heat transfer field is related to the number of layers of the multi-layer heat transfer field.

Based on the relationship between the field strength distribution at both ends and the center position along axial heat transfer field and parameter value (l/r) of heat transfer field, it can be known that for the general case, if the field distributed in the heat transfer field meets the even characteristic, the general values of field can be calculated as follows:

$$\Phi = B_0 A = \frac{\mu_0 n I A}{2l} \,. \tag{10}$$

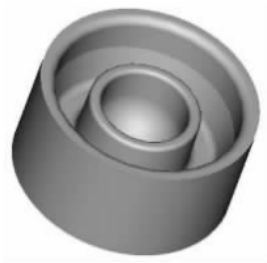

Fig. 1. Shape of workpiece

4. Experimental analysis

4.1. Models and parameters

The shape of the workpiece is as shown in Fig. 1 and due to the symmetry of the workpiece, we use its 1/8 for analysis.

Initial conditions: the material of blank is 6061 aluminum alloy whose stress-strain curve at various temperature is shown in Figure 2; the blank is heated to the initial forging temperature which is 480°, with the resistance-heated furnace; the blank is the bar, the size of which is; the surrounding medium temperature is 20°. The entire simulation process includes several following parts:

(1) The blank is removed from the furnace to the anvil, during the process of which there is no plastic deformation and only thermal conversion. Data required for simulation: it takes 10s for the blank to be removed from the furnace to the anvil. (2) The blank stays on the anvil, the process of which is the same as it in (1), with only thermal conversion. Data required: the blank stays on the anvil for 2s, the temperature of anvil is 300° (putting the iron burnt red on the anvil can preheat the anvil) and free resting=0.003 is selected for heat transfer coefficient. (3) The process for blank to be removed from anvil to mould is the same as it in (1), with only thermal conversion. Data required: it takes 6s to remove blank from anvil to mould. (5) The process of forging forming is the same as it in (3), where there is plastic deformation and also thermal conversion. Data required: the mould temperature is 400°, but the remaining conditions are the same as it in (3).

4.2. Results and analysis

It can be seen from Fig. 2 that the bulk temperature of the blank is reduced from 480°C to about 450°C due to the time taken to remove the blank from the furnace to upsetting, and the surface is in contact with the air so that the central temperature is slightly higher than the temperature on the surface.

As can be seen from Figure 4, the internal strain of the forging is uneven: the deformation at the bottom of workpiece is small and the equivalent strain is about 1; when the blank is formed, the upper part is back-extruded into two rings, so the deformation at the top of the workpiece is large and the equivalent strain is about 2; the burr part is intensely deformed at the external rim, and the equivalent defor-

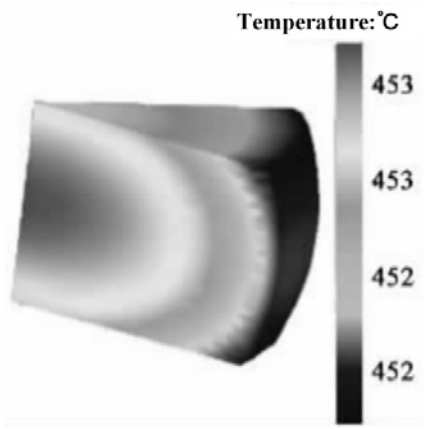

Fig. 2. Temperature distribution after upsetting

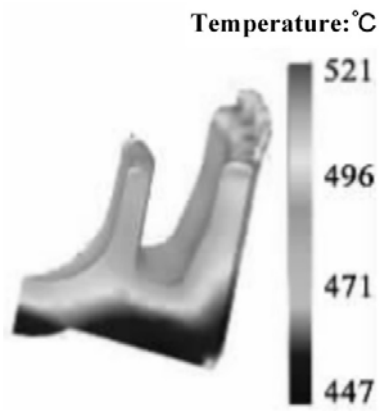

Fig. 3. Temperature distribution after forming of forging

mation reaches 2.91. From the point of view of the equivalent stress distribution, the distribution of its values is more even, mostly between 40 and 60 MPa, and the stress in the burr parts is larger, which is more than 95 MPa.

The required pressure for forming the upsetting and forging of this workpiece can be predicted from Fig. 5, in which the crest in the front is the forming pressure required by upsetting of workpiece, about 6500 N, but due to the use of the 1/8 model analysis, it needs to be multiplied by 8, about 52 000 N. Similarly, the forging forming pressure worked out is 208 000 N.

5. Conclusion

A finite element analysis method of aluminum alloy plastic flow thermally coupled welding process is proposed in the Paper and the basic theory of finite element for rigid viscoplasticity of aluminum alloy and the analysis model of finite element field

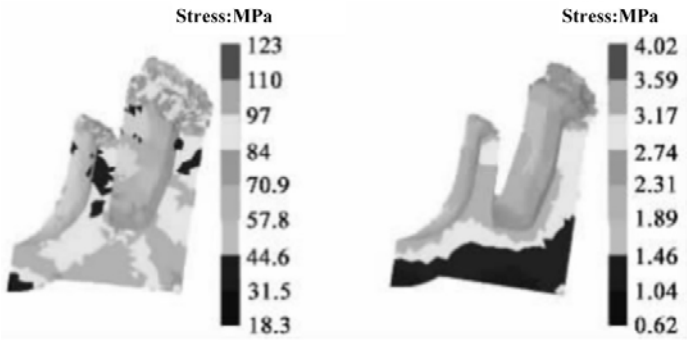

Fig. 4. Equivalent stress-strain distribution diagram

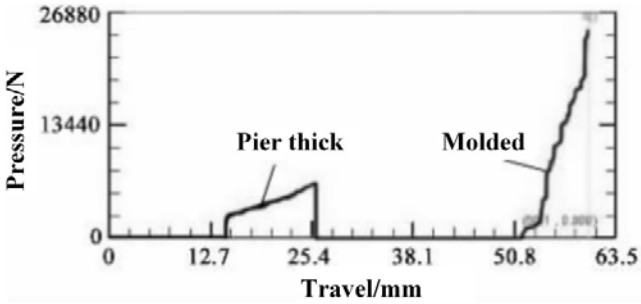

Fig. 5. Forming pressure diagram

for aluminum alloy plastic flow thermal coupling are given. The effectiveness of the algorithm has been verified through the simulation experiment, which has improved the research and analysis precision of aluminum alloy plastic flow thermally coupled welding process. The main research direction of the Paper in the next step mainly includes the performance improvement of finite element analysis algorithm, and the extension of type analysis on aluminum alloy component.

Acknowledgement

Shandong Province Key Projects of Research and Development (2016GNC112006).

References

[1] Yin P F, Zhang R, Xiong J T, et al.: (2013) *Numerical simulation of coupled thermo-mechanical process of friction stir welding in quasi-steady-state*[J]. Acta Physica Sinica, 62(1):709-712.

[2] Cui J H, Xu W, Guo Z H: (2013) *Coupled Thermo-Flowing 3D Steady State Model of Friction Stir Welding Process*[J]. Applied Mechanics & Materials, 470:325-329.

[3] Dong X, Xiangfeng L I, Zuo D, et al.: (2011) *Numerical analysis of heat transfer*

and plastic flow during friction stir welding process of aluminum alloy[J]. Ordnance Material Science & Engineering, 34(5):44-48.

[4] Zhu Z, Wang M, Zhang H J, et al.: (2016) *Simulation on Temperature Field of Friction Stir Welding of 2A14 Aluminum Alloy Based on Equivalent Film Method*[J]. Key Engineering Materials, 2016, 723.

[5] Liu X, Chen G, Ni J, et al.: (2017) *Computational Fluid Dynamics Modeling on Steady-State Friction Stir Welding of Aluminum Alloy 6061 to TRIP Steel*[J]. 139(5):051004.

[6] Mishra R, Mahoney M W, Sato Y, et al.: (2013) *A Coupled Thermal/Material Flow Model of Friction Stir Welding Applied to Sc-Modified Aluminum Alloys*[M]// Friction Stir Welding and Processing VII. Springer International Publishing, 2013:1730-1740.

[7] Ji H K, Barlat F, Kim C, et al.: (2009) *Themo-mechanical and microstructural modeling of friction stir welding of 6111-T4 aluminum alloys*[J]. Metals and Materials International, 15(1):125-132.

[8] Chiumenti M, Dialami N, Ponthot J P, et al.: (2013) *Visualization of material flow for friction stir welding processes simulation*[C]// PLASTICITY 2013, International Symposium on PLASTICITY and ITS Current Applications, Nassau, Bahamas, 3-8 January.

[9] Hamilton C, Kopyściańki M, Senkov O, et al.: (2013) *A Coupled Thermal/Material Flow Model of Friction Stir Welding Applied to Sc-Modified Aluminum Alloys*[J]. Metallurgical and Materials Transactions A, 44(4):1730-1740.

[10] Guo Z H, Zhao G Y, Ke L M, et al.: (2011) *Thermo-Mechanical Coupled Analysis of Deformation Behavior in Friction Stir Welding Process of Aluminum 7075 Plate with Conical Pin*[J]. Advanced Materials Research, 338:618-621.

[11] Chiumenti M, Cervera M, Saracibar C A D, et al.: (2013) *Numerical modeling of friction stir welding processes*[J]. Computer Methods in Applied Mechanics & Engineering, 254(2):353–369.

[12] Lu H, Li P, Xu Z, et al.: (2012) *The Influence of Thread Form on Refilling Friction Stir Welding of 2219 Aluminum Alloy Sheets*[J]. Transactions of Jwri, 2011:41-42.

[13] Hamilton C, Węlowski M S, Dymek S, et al.: (2015) *Using a Coupled Thermal/Material Flow Model to Predict Residual Stress in Friction Stir Processed AlMg9Si*[J]. Journal of Materials Engineering and Performance, 24(3):1305-1312.

[14] Vijayan D, Rao V S: (2014) *Friction Stir Welding of Age-Hardenable Aluminum Alloys: A Parametric Approach Using RSM Based GRA Coupled With PCA*[J]. Journal of The Institution of Engineers (India): Series C, 95(2):127-141.

[15] Guo Z H, Zhao G Y, Ke L M, et al.: (2011) *A 3D Coupled Thermo-Mechanical FE Model for Friction Stir Welding of 7075 Aluminum Alloy Plate*[J]. Advanced Materials Research, 314-316:346-350.

Received May 7, 2017